MOLECULAR IMAGING AND BIOLOGY

Mol Imaging Biol (2019) 21:348–355
DOI: 10.1007/s11307-018-1248-1

Published Online: 9 July 2018

RESEARCH ARTICLE

Differentiation of Malignant and Benign Head and Neck Tumors with Amide Proton Transfer-Weighted MR Imaging

Lu Yu,[1,2] Chunmei Li,[1] Xiaojie Luo,[1] Jinyuan Zhou,[3] Chen Zhang,[1] Yi Zhang,[4] Min Chen[1,2]

[1]*Department of Radiology, Beijing Hospital, National Center of Gerontology, No. 1 Da-Hua Road, Dong Dan, Beijing, 100730, China*
[2]*Graduate School of Peking Union Medical College, No. 9 Dong Dan San Tiao, Beijing, 100730, China*
[3]*Department of Radiology, Johns Hopkins University, 600 N. Wolfe Street, Park 336, Baltimore, MD, 21287, USA*
[4]*Center for Brain Imaging Science and Technology, Key Laboratory for Biomedical Engineering of Ministry of Education, College of Biomedical Engineering & Instrument Science, Zhejiang University, No. 388 Yuhangtang Road, Hangzhou, 310058, Zhejiang, China*

Abstract

Purpose: To prospectively evaluate the feasibility and capability of amide proton transfer-weighted (APTw) imaging for the characterization of head and neck tumors.

Procedures: Twenty-nine consecutive patients with suspected head and neck tumors were enrolled in this study and underwent APTw magnetic resonance imaging (MRI) on a 3.0-T MRI scanner. The patients were divided into malignant ($n = 16$) and benign ($n = 13$) groups, based on pathological results. A map of magnetization transfer ratio asymmetry at 3.5 ppm [MTR_{asym} (3.5 ppm)] was generated for each patient. Interobserver agreement was evaluated and comparisons of MTR_{asym} (3.5 ppm) were made between the malignant and benign groups. Receiver operating characteristic analysis was used to determine the appropriate threshold value of MTR_{asym} (3.5 ppm) for the differentiation of malignant from benign tumors.

Results: The intraclass correlation coefficients of the malignant and benign groups were 0.96 and 0.90, respectively, which indicated a good interobserver agreement. MTR_{asym} (3.5 ppm) was significantly higher for the malignant group (3.66 ± 1.15 %) than for the benign group (1.94 ± 0.93 %, $P < 0.001$). APTw MRI revealed an area under the curve of 0.904 in discriminating these two groups, with a sensitivity of 81.3 %, a specificity of 92.3 %, and an accuracy of 86.2 %, at the threshold of 2.62 % of MTR_{asym} (3.5 ppm).

Conclusions: APTw MRI is feasible for use in the head and neck tumors and is a valuable imaging biomarker for distinguishing malignant from benign lesions.

Key words: APTw imaging, CEST imaging, Head and neck tumors, MRI

Introduction

Head and neck cancer is the seventh most frequent cancer and the ninth most frequent cause of death from cancer [1]. The overall survival rate of patients with head and neck cancers has not increased much over recent years, although oncological treatments have achieved great advances [2, 3]. Head and neck tumors are of variable types, and the characteristics of these tumors affect the prognosis and the appropriate treatment strategy. Thus, it is of the utmost importance to make an accurate diagnosis. Many advanced MR imaging techniques, such as diffusion-weighted imaging (DWI), dynamic contrast-enhanced (DCE) magnetic resonance imaging (MRI), and

Correspondence to: Min Chen; *e-mail:* cjr.chenmin@vip.163.com

positron emission tomography (PET)/MR, have been used in the diagnosis of head and neck tumors and can provide much information about the underlying biology [4–6]. However, the differentiation between benign and malignant head and neck tumors remains problematic with these techniques. DWI often suffers from susceptibility artifacts, and the accuracy of apparent diffusion coefficient (ADC) values is affected by the choice of *b* values. DCE-MRI provides perfusion and permeability information through the injection of gadolinium (Gd), but this technique is limited in those lesions with an intact blood-brain barrier [7], which can lead to high false-negative and false-positive results. PET/MR is usually restricted by the length of the scan time and the cost but serves as an alternative to PET/CT in the clinical workup [8, 9].

Since the early 2000s, amide proton transfer-weighted (APTw) MR imaging has emerged as an important contrast mechanism for MRI in the field of molecular imaging [10]. Based on the chemical exchange saturation transfer (CEST) mechanism, the technique can indirectly detect mobile proteins and peptides in tissues [10], such as those in the cytoplasm, through the exchange between amide protons and bulk water protons, without an exogenous contrast agent. Numerous previous studies have shown that APTw imaging can largely improve the diagnostic performance in brain tumors, compared with conventional, structural MRI sequences [11, 12]. Some preliminary studies have also applied APTw imaging to other cancers, such as those in the prostate [13], breast [14], liver [15], and lung [16]. However, to our knowledge, no studies have been reported that were designed to evaluate the clinical potential of APTw MRI in the diagnosis of head and neck tumors.

In this study, we hypothesized that malignant tumors have a high cell proliferation index and more mobile proteins and peptides to undertake cellular activities. The associated APTw signal could then be increased compared with benign tumors and normal tissues [13, 16]. Due to this effect, the application of APTw MRI could thus improve the diagnostic performance in head and neck tumors. Therefore, the main goal of this study was to investigate the feasibility of APTw MRI to characterize various head and neck tumors on a 3.0 T and to evaluate the clinical potential of this method to differentiate malignant tumors from benign lesions.

Materials and Methods

Subjects

The local institutional review board approved this study and all participants gave written informed consent before enrolling. Between September 2016 and December 2017, 35 consecutive adult inpatients and outpatients with suspected head and neck tumors were recruited for this study. These subjects were referred for imaging for various indications. The inclusion criteria were as follows: (1) no previous treatment; (2) all pathological examinations of specimens were obtained by means of surgical resection, biopsy, and/or follow-up examinations; (3) APTw MR imaging was acquired before surgical resection and biopsy, and the interval was not more than 4 weeks; and (4) image quality was adequate for analysis. Based on the inclusion criteria, three patients were excluded from this study because of the absence of pathological results. In addition, the data from three patients were further rejected because of insufficient image quality due to obvious motion artifacts. Finally, a total of 29 patients (14 men, 15 women; age, 52.0 ± 18.1 years old) with suspected head and neck tumors were chosen for the data analysis in this study. All patients were divided into the malignant ($n = 16$) or the benign ($n = 13$) group according to the pathological results, as shown in Table 1.

Image Acquisition

All MR imaging was performed on a 3.0-T MR system (Achieva 3.0 T, Philips Medical Systems, Best, the Netherlands), using a dual-channel body coil for signal transmission and a 16-channel head and neck coil for signal reception. Conventional structural MRI sequences, including axial T2-weighted imaging (T2WI) with fat suppression, sagittal T2WI, coronal T2WI, axial T1-weighted imaging (T1WI), and DWI, were scanned for reference.

An APTw pulse sequence was employed, based on one T2WI image slice that showed the maximum area of the tumor. This was based on a single-shot, turbo-spin-echo readout: repetition time, 3 s; turbo-spin-echo factor, 54; field of view, 230 mm × 221 mm; matrix, 105 × 100 (reconstructed to be 400 × 400); and slice thickness, 6 mm. We used a pulse-train radiofrequency (RF) irradiation (saturation duration, 200 ms × 4; inter-pulse delay, 10 ms; power level, 2 μT), as developed previously [17]. The APTw imaging was performed with a multi-offset, multi-acquisition protocol. The 31 offsets were 0, ± 0.25, ± 0.5, ± 0.75, ± 1, ± 1.5, ± 2, ± 2.5, ± 3.0 (2), ± 3.25 (4), ± 3.5 (8), ± 3.75 (4), ± 4 (2), ± 4.5, ± 5.0, and ± 6.0 ppm, and the values in parentheses were the number of acquisitions, which was 1 if not specified

Table 1. Demographic information, clinical symptoms, and pathological results

Characteristics	Value
Age (mean ± SD)	52.0 ± 18.1 years
Gender (ratio)	
Female	15/29
Male	14/29
Clinical symptoms (ratio)	
Head and neck mass	12/29
Epistaxis	6/29
Hearing loss	2/29
Others	9/29
Pathological results (ratio)	
Nasopharyngeal carcinoma	7/29
Metastatic carcinoma	5/29
Lymphoma	2/29
Schwannoma	3/29
Lipoma	1/29
Others	11/29

[18]. This combined APTw/Z-spectrum acquisition method avoided the prescan between the APTw image scan and the Z-spectrum scan, which can affect the shim and frequency offset settings. In addition, an unsaturated image and a saturated image at 15.6 ppm (2 kHz) were acquired for signal normalization and for the calculation of the MTR value associated with conventional magnetization transfer (MT) imaging [19]. So we further defined MTR (15.6 ppm) to characterize MT effects. The patients were instructed to limit swallowing and their heads were immobilized with sponge. The total acquisition time for the APTw imaging procedure was 4 min and 21 s. The duration of a complete MR examination was about 18 min.

APTw Image Processing

The image analysis was performed using the Interactive Data Language (IDL, ITT Visual Information Solutions, Boulder, CO, USA). The normalized saturated signal intensity curve (usually called the Z-spectrum) was calculated with 31 different frequency offsets (−6 to 6 ppm). Then, the measured Z-spectrum was fitted on a pixel-by-pixel basis, and the B0 inhomogeneity map was created. After this, the original Z-spectrum was corrected for the B0 inhomogeneity effects through the interpolation and centering of the Z-spectrum, as previously reported [20, 21]. As usual, the magnetization transfer ratio asymmetry (MTR_{asym}) was defined as follows: $MTR_{asym}(\text{offset}) = S_{sat}(-\text{offset}) / S_0 - S_{sat}(+\text{offset}) / S_0$, in which S_{sat} and S_0 are the signal intensities with and without selective RF irradiation, respectively. Specifically, the APTw signal was calculated based on the MTR_{asym} at 3.5 ppm: $MTR_{asym}(3.5\ \text{ppm}) = S_{sat}(-3.5\ \text{ppm}) / S_0 - S_{sat}(+3.5\ \text{ppm}) / S_0$. MTR_{asym} was defined to characterize CEST effects. In this study, the APTw images were displayed by rainbow colors and a display window (−5 %, 5 %) was used. In addition, we measured the total MTR_{asym} signal by integrating the MTR_{asym} spectrum over the frequency offset range from 1 to 4 ppm.

Image analysis was performed by two neuroradiologists (reader 1, CL, and reader 2, LY, who have 10 and 5 years of experience in imaging diagnosis, respectively, and who were blind to the final pathological results and the other's findings). Regions of interest (ROIs) were manually outlined on the whole tumor by the two neuroradiologists. The T2WI image was used as the anatomical reference to draw the ROI. Large cystic cavities, large areas of liquefactive necrosis, calcification, or hemorrhage, or large vessels evident on standard structural MRI sequences, were always excluded from the ROI selection [22, 23].

Statistical Analysis

All data were analyzed using the statistical package SPSS 20.0. The results were expressed as mean ± standard deviation (SD). Interobserver agreement between reader 1 and reader 2 was examined by using the intraclass correlation coefficients (ICC). An ICC value greater than 0.75 was considered a good agreement. Levene's test was used for the homogeneity of variance test. Then, the independent sample Student's *t* test was performed to evaluate the differences in MTR_{asym} (3.5 ppm) and other MRI parameters between the malignant and benign groups. Finally, receiver operating characteristic (ROC) analysis was performed to determine the appropriate feasible threshold value for the differentiation of the malignant from the benign group. The sensitivity, specificity, and accuracy were calculated, and the best threshold value was determined by maximizing the sum of sensitivity and specificity. In

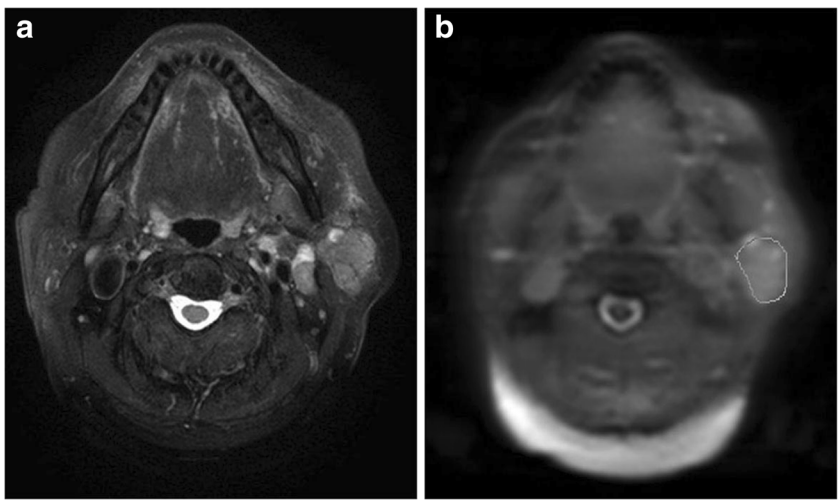

Fig. 1. A representative ROI defined for quantitative analysis. An ROI was manually outlined on the tumor with the anatomical reference from the T2WI image. **a** T2WI image and **b** MTR image.

addition, P values lower than 0.05 were considered statistically significant.

Results

The demographic information, clinical symptoms, and pathological results for all patients are summarized in Table 1. The representative ROI chosen for quantitative analysis is shown in Fig. 1.

Feasibility of APTw Imaging in Head and Neck Tumors

The ICCs of MTR_{asym} (3.5 ppm) between two readers were 0.96 and 0.90 for the malignant and benign groups, respectively, which indicated a good interobserver agreement. Figure 2 shows the MTR_{asym} (3.5 ppm) signals of the malignant and benign groups for reader 1 and reader 2. A significant difference was found between the malignant group and the benign group for both reader 1 and reader 2 ($P < 0.01$). There was an exception in the case of the lipoma (Fig. 2), in which MTR_{asym} (3.5 ppm) was 0.24 % for reader 1 and −0.74 % for reader 2, and the mean MTR_{asym} (3.5 ppm) was −0.25 %.

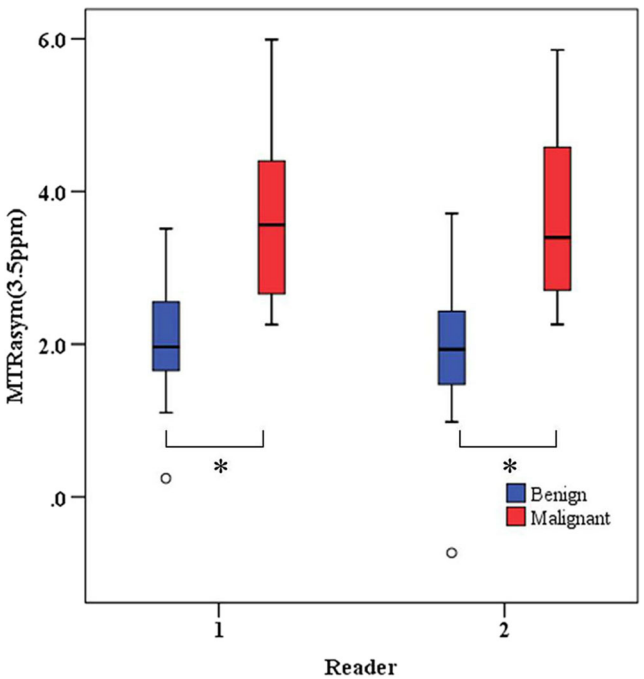

Fig. 2. The MTR_{asym} (3.5 ppm) of the benign and malignant groups for the two readers. A significant difference was observed between the malignant group and the benign group for both reader 1 and reader 2. The MTR_{asym} (3.5 ppm) of the lipoma was 0.24 % for reader 1 and −0.74 % for reader 2. *$P < 0.01$

Comparisons Between the Benign and Malignant Groups

Figure 3 shows the ROI-averaged Z-spectra and the corresponding MTR_{asym} spectra for the benign and malignant groups. The Z-spectra shape for both groups was very smooth in the offset range from −6 to 6 ppm. The Z-spectrum (−6 to 6 ppm) of the malignant group was higher than that of the benign group (Fig. 3a), but there was no significant difference. The effects of conventional MT and direct water saturation dominate the Z-spectra. The upward shift in the Z-spectra for malignant tumors may be attributable to many factors, such as increased water content and increased macromolecular mobility in the regions [20]. Because the sample size of the benign group was relatively small and the benign group had more variable pathological results, such as lipoma, which had the lowest MTR_{asym} (3.5 ppm), the Z-spectrum of the malignant group showed a smaller standard deviation compared with the benign group (Fig. 3a). The MTR_{asym} (3.5 ppm) was significantly higher for the malignant group (3.66 ± 1.15 %) than for the benign group (1.94 ± 0.93 %, $P < 0.001$) (Fig. 3b). There was a notable CEST effect from 1 to 4 ppm in both the malignant and benign groups. The total MTR_{asym} signal of the malignant group was significantly higher than that of the benign group (7.40 ± 2.20 *vs.* 3.92 ± 2.70 %, $P = 0.001$) (Fig. 4). However, there was no significant difference in the MTR (15.6 ppm) between the malignant and benign groups (18.40 ± 3.55 *vs.* 18.11 ± 9.41 %, $P = 0.91$).

Figure 5 shows two examples of T2WI, T1WI, APTw image, and a hematoxylin and eosin (H&E)-stained pathological section of nasopharyngeal carcinoma and schwannoma, corresponding to the malignant and benign groups, respectively. The APTw intensity of the nasopharyngeal carcinoma (3.12 %) was higher than that of the schwannoma (2.54 %). In addition, the core and peripheral portions of the tumor on APTw images were not homogeneous.

ROC Analysis

Figure 6 illustrates the ROC curves that used the APTw imaging to differentiate the malignant from the benign group. APTw demonstrated an area under the curve (AUC) of 0.904 in discriminating these two groups, with a sensitivity of 81.3 %, a specificity of 92.3 %, and an accuracy of 86.2 %, at the threshold MTR_{asym} (3.5 ppm) of 2.62 %.

Discussion

We evaluated the characteristics of head and neck tumors using APTw MR imaging in 29 patients. We obtained good interobserver agreement and found significant correlation. In addition, due to the significant differences revealed between

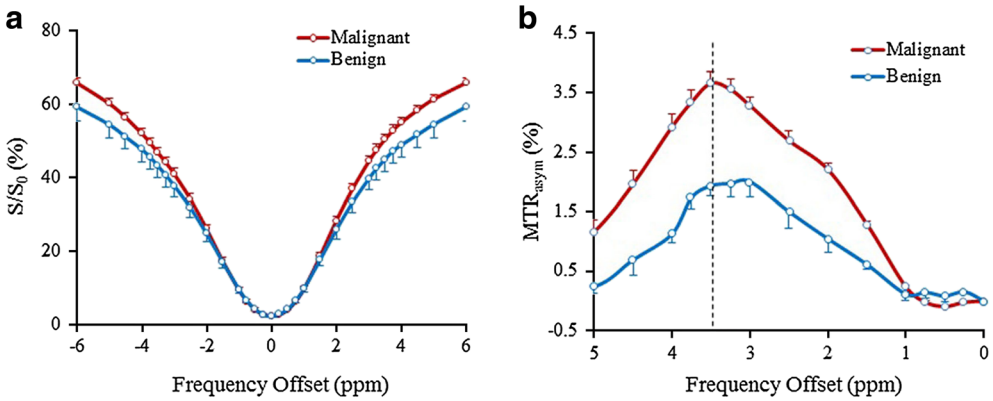

Fig. 3. The Z-spectra (– 6 to 6 ppm) and MTR_{asym} spectra of the malignant and benign groups. **a** The Z-spectrum was higher in the malignant group than in the benign group. **b** The MTR_{asym} (3.5 ppm) of the malignant group was higher than that of the benign group ($P < 0.001$).

malignant and benign tumors, APTw imaging could be used to differentiate malignant from benign head and neck tumors. Therefore, our current study demonstrated the value of APTw imaging in the diagnosis of head and neck tumors.

Prior to our study, Yuan et al. for the first time, applied APTw MR imaging in normal tissue of the head and neck in healthy volunteers and measured the Z-spectra and APTw signals quantified by the MTR_{asym} (3.5 ppm) of the masseter muscle, parotid glands, submandibular glands, and thyroid glands [24]. This study demonstrated the feasibility and repeatability of APTw MRI on clinical MRI scanners for normal head and neck tissue. And the composition differences could lead to different APTw signals. By et al. and Dula et al. implemented APTw CEST in the cervical spinal cord of healthy controls and multiple sclerosis cohorts on 3.0 T and 7.0 T [25, 26]. The results of those studies provided biochemical information about disease processes within the cervical spinal cord. In addition, Wang et al. used CEST imaging to investigate glucose uptake and the metabolism of head and neck cancer on a clinical 3.0-T MRI scanner [27]. Based on these previous studies, our work applied APTw MRI to further detect head and neck tumors and proved the clinical potential.

APTw MRI has been widely used in brain tumors. In addition, APTw signals have shown significant differences between malignant and benign lesions in patients with prostatic [13], thoracic [16], and breast tumors [28]. This technique could provide indirect acquisition of signal intensity through the chemical exchange between amide protons in mobile proteins and peptides and bulk water protons [10]. The effect of APT is influenced by protein content and intracellular pH changes [29, 30]. In tumors, the

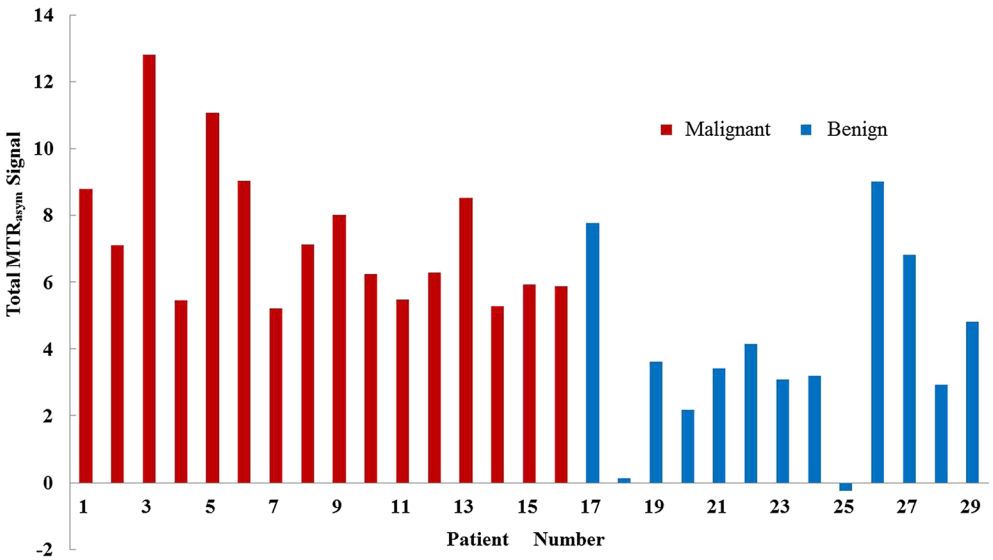

Fig. 4. The total MTR_{asym} signal from 1 to 4 ppm of all patients for both groups. There was a significant difference in the total MTR_{asym} signal between the malignant and benign groups.

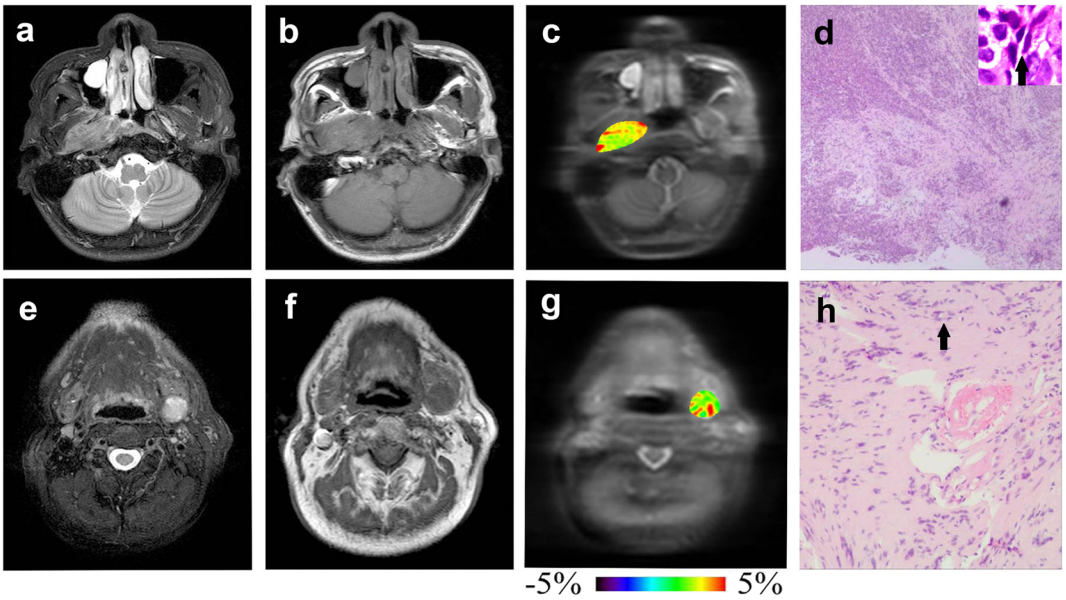

Fig. 5. Conventional and APTw images of representative malignant and benign tumors. **a** T2WI, **b** T1WI, **c** APTw, and **d** H&E-stained pathological section (original magnification ×40 and ×400, black arrow: tumor cells) for a 21-year-old male patient with nasopharyngeal carcinoma. The average MTR_{asym} (3.5 ppm) signal of the tumor was 3.12 %. **e** T2WI, **f** T1WI, **g** APTw, and **h** H&E-stained pathological section (original magnification ×100, black arrow: Schwann cells) for an 81-year-old-male patient with schwannoma. The average MTR_{asym} (3.5 ppm) of the tumor was 2.54 %.

intracellular pH level normally remains almost unchanged, and the observed APTw signal is mainly dominated by the endogenous protein and peptide content. In malignant tumors, the mobile proteins and peptides are more abundant than in benign tumors and normal tissue.

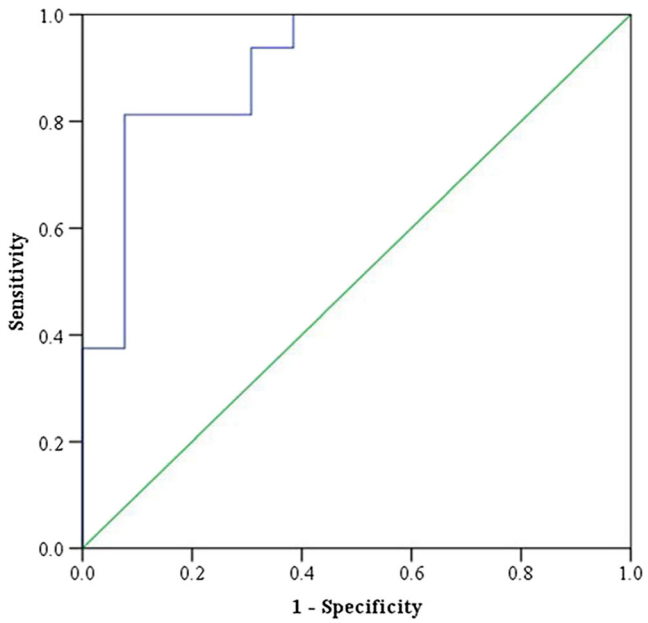

Fig. 6. The ROC analysis. MTR_{asym} (3.5 ppm) can be used as an imaging biomarker to distinguish malignant tumors from benign lesions at the threshold of 2.62 %.

Previous studies have demonstrated that APTw imaging could not only differentiate high-grade glioma from low-grade glioma without intense contrast enhancement but also direct stereotactic biopsy [23]. APTw imaging has also been applied to distinguish true progression from treatment response in brain tumors [31–33]. In our study, MTR_{asym} (3.5 ppm) was significantly higher for malignant tumors than for benign lesions. The mean MTR_{asym} (3.5 ppm) of four head and neck tumors ranged from 1.2 to 3.2 %, enough to be distinguishable from surrounding normal tissues in a previous study [24]. We recruited more patients with malignant and benign head and neck tumors. Further, we found that there were significant differences in MTR_{asym} (3.5 ppm) between the two groups, indicating the mobile proteins and peptide differences in these two kinds of lesions. However, the difference in the MTR (15.6 ppm) between the two groups in this study was not statistically significant, and the lower RF saturation power (2 μT) used in our protocol may have caused this inconsistency [19]. We found a significant difference of total MTR_{asym} from 1 to 4 ppm between the two groups. We chose this range to calculate the total CEST signal because we wanted to include APT at 3.5 ppm, possible amine CEST at 3 ppm, creatine CEST at 2 ppm, and possible glucose CEST at 1 ppm. In addition, the MTR_{asym} spectrum over this range was relatively stable and free of artifacts. The difference is due to the increased cellularity and material metabolism in malignant tumors compared with benign lesions [27].

We recommend MTR_{asym} (3.5 ppm) and total MTR_{asym} to differentiate the two groups. MTR_{asym} (3.5 ppm) reflects

the difference of endogenous, low concentration mobile proteins, and peptides in tissues between malignant and benign groups. Total MTR_{asym} was used to evaluate the total CEST signal intensity of the two groups under the MTR curve. In addition, a significant difference was observed in MTR_{asym} (3.5 ppm) and total MTR_{asym} between the malignant and the benign group in our study. There was no significant difference in MTR (15.6 ppm) between the two groups.

We also observed a distinctive MTR_{asym} (3.5 ppm) for lipoma, which contained a fraction of negative MTR_{asym} values. It was different from other benign lesions. Lipoma is caused by hyperplasia of normal fat because of gene mutation and contains a large amount of mature adipocytes, which are somewhat larger than those found in ordinary fat at microscopic pathology. The hypointensity of lipoma on APTw imaging results from relatively rare proteins and peptides.

The threshold MTR_{asym} (3.5 ppm) was 2.62 % for the differentiation of benign from malignant head and neck tumors. The optimal cutoff value for differentiating the tumor progression from treatment-related effects in glioblastoma was demonstrated in a previous study [32]. Yoshiharu et al. [34] also found a feasible threshold value for the differential diagnosis between malignant and benign pulmonary nodules. Our finding of feasible threshold values demonstrated the capabilities of APTw MR imaging in the head and neck, which indicated the potential of APTw MRI for clinical application.

Due to air flow in the pharyngeal cavity and the complicated anatomical structures in the head and neck, APTw images of this region could be much more heterogeneous than in the brain. We took measures to improve the quality of APTw images, such as fixing the patients' heads and limiting swallowing. In a previous study of brain tumors, an ROI was manually drawn to include a whole tumor area and avoid areas with large cystic cavities, large liquefactive necrosis, calcification, large vessels, and hemorrhages [22, 23]. In our study, we used the same method to avoid possible artifacts when choosing the ROI. MTR_{asym} is higher in acute hemorrhage than in the solid components of tumors and the MTR_{asym} of acute hemorrhage differs from that of subacute hemorrhage, so we excluded hemorrhage to avoid its effect on the tumor [35].

There are several limitations to our study. First, the patient population was a collection of diverse lesions in different regions of the head and neck. There were only one or two cases of certain tumors that may have affected the MTR_{asym}. In addition, there was no detailed analysis of the pathologic features, such as the proliferation index and microvascular density. A large prospective cohort study that includes detailed pathologic information about each lesion is needed. Second, the applied APTw imaging allowed only one single-slice acquisition. We chose the maximum slice on T2WI images of the tumor to obtain the APTw images. A 3D imaging acquisition sequence has been reported in the brain [17, 36] and thus could also be used in the head and neck. Finally, the APTw signal using an asymmetry analysis can be affected by some other factors, such as the background semi-solid magnetization transfer asymmetry effect and the NOE of aliphatic protons [37]. To more accurately quantify the APT effect, a more fully developed APTw imaging acquisition or analysis approach is needed in the future [38].

Conclusions

APTw MR imaging could be used to detect and characterize tumors of the head and neck on a 3.0-T MR system. In addition, this technique has also shown clinical potential to noninvasively distinguish malignant tumors from benign tumors in the head and neck.

Acknowledgments. This study was supported by grants from the National Natural Science Foundation of China (81361120392, 81401404, and 81771826), Beijing Municipal Natural Science Foundation (7154235), and the National Institutes of Health (R01CA166171, R01CA228188).

Compliance with Ethical Standards

Conflict of Interest

The authors declare that they have no conflict of interest.

References

1. Stewart BW, Wild CP (2014) World cancer report 2014. WHO Press, Lyon, p 423
2. Siegel RL, Miller KD, Jemal A (2017) Cancer statistics, 2017. CA Cancer J Clin 67:7–30
3. Siegel RL, Miller KD, Jemal A (2018) Cancer statistics, 2018. CA Cancer J Clin 68:7–30
4. Jansen JFA, Parra C, Lu Y, Shukla-Dave A (2016) Evaluation of head and neck tumors with functional MR imaging. Magn Reson Imaging Clin N Am 24:123–133
5. Razek AA, Elsorogy LG, Soliman NY et al (2011) Dynamic susceptibility contrast perfusion MR imaging in distinguishing malignant from benign head and neck tumors: a pilot study. Eur J Radiol 77:73–79
6. Abdel Razek AA, Samir S, Ashmalla GA (2017) Characterization of parotid tumors with dynamic susceptibility contrast perfusion-weighted magnetic resonance imaging and diffusion-weighted MR imaging. J Comput Assist Tomogr 41:131–136
7. Sun H, Xin J, Zhou J, Lu Z, Guo Q (2018) Applying amide proton transfer MR imaging to hybrid brain PET/MR: concordance with gadolinium enhancement and added value to [^{18}F]FDG PET. Mol Imaging Biol 20:473–481
8. Galgano SJ, Marshall RV, Middlebrooks EH, McConathy JE, Bhambhvani P (2018) PET/MR imaging in head and neck cancer: current applications and future directions. Magn Reson Imaging Clin N Am 26:167–178
9. Ruhlmann V, Ruhlmann M, Bellendorf A, Grueneisen J, Sawicki LM, Grafe H, Forsting M, Bockisch A, Umutlu L (2016) Hybrid imaging for detection of carcinoma of unknown primary: a preliminary comparison trial of whole-body PET/MRI versus PET/CT. Eur J Radiol 85:1941–1947
10. Ward KM, Aletras AH, Balaban RS (2000) A new class of contrast agents for MRI based on proton chemical exchange dependent saturation transfer (CEST). J Magn Reson 143:79–87
11. Zhang J, Zhu W, Tain R, Zhou XJ, Cai K (2018) Improved differentiation of low-grade and high-grade gliomas and detection of tumor proliferation using APT contrast fitted from Z-spectrum. Mol Imaging Biol. https://doi.org/10.1007/s11307-017-1154-y

12. Zhou J, Zhu H, Lim M, Blair L, Quinones-Hinojosa A, Messina SA, Eberhart CG, Pomper MG, Laterra J, Barker PB, van Zijl PCM, Blakeley JO (2013) Three-dimensional amide proton transfer MR imaging of gliomas: initial experience and comparison with gadolinium enhancement. J Magn Reson Imaging 38:1119–1128
13. Jia G, Abaza R, Williams JD et al (2011) Amide proton transfer MR imaging of prostate cancer: a preliminary study. J Magn Reson Imaging 33:647–654
14. Klomp DW, Dula AN, Arlinghaus LR et al (2013) Amide proton transfer imaging of the human breast at 7T: development and reproducibility. NMR Biomed 26:1271–1277
15. Chen SZ, Yuan J, Deng M, Wei J, Zhou J, Wáng YXJ (2016) Chemical exchange saturation transfer (CEST) MR technique for in-vivo liver imaging at 3.0 tesla. Eur Radiol 26:1792–1800
16. Ohno Y, Yui M, Koyama H, Yoshikawa T, Seki S, Ueno Y, Miyazaki M, Ouyang C, Sugimura K (2016) Chemical exchange saturation transfer MR imaging: preliminary results for differentiation of malignant and benign thoracic lesions. Radiology 279:578–589
17. Zhu H, Jones CK, van Zijl PCM, Barker PB, Zhou J (2010) Fast 3D chemical exchange saturation transfer (CEST) imaging of the human brain. Magn Reson Med 64:638–644
18. Song G, Li C, Luo X, Zhao X, Zhang S, Zhang Y, Jiang S, Wang X, Chen Y, Chen H, Gong T, Zhou J, Chen M (2017) Evolution of cerebral ischemia assessed by amide proton transfer-weighted MRI. Front Neurol 8(67)
19. Li C, Peng S, Wang R, Chen H, Su W, Zhao X, Zhou J, Chen M (2014) Chemical exchange saturation transfer MR imaging of Parkinson's disease at 3 Tesla. Eur Radiol 24:2631–2639
20. Zhou J, Blakeley JO, Hua J, Kim M, Laterra J, Pomper MG, van Zijl PCM et al (2008) Practical data acquisition method for human brain tumor amide proton transfer (APT) imaging. Magn Reson Med 60:842–849
21. Wen Z, Hu S, Huang F, Wang X, Guo L, Quan X, Wang S, Zhou J (2010) MR imaging of high-grade brain tumors using endogenous protein and peptide-based contrast. Neuroimage 51:616–622
22. Yu H, Lou H, Zou T, Wang X, Jiang S, Huang Z, du Y, Jiang C, Ma L, Zhu J, He W, Rui Q, Zhou J, Wen Z (2017) Applying protein-based amide proton transfer MR imaging to distinguish solitary brain metastases from glioblastoma. Eur Radiol 27:4516–4524
23. Jiang S, Eberhart CG, Zhang Y, Heo HY, Wen Z, Blair L, Qin H, Lim M, Quinones-Hinojosa A, Weingart JD, Barker PB, Pomper MG, Laterra J, van Zijl PCM, Blakeley JO, Zhou J (2017) Amide proton transfer-weighted magnetic resonance image-guided stereotactic biopsy in patients with newly diagnosed gliomas. Eur J Cancer 83:9–18
24. Yuan J, Chen S, King AD, Zhou J, Bhatia KS, Zhang Q, Yeung DKW, Wei J, Mok GSP, Wang YX (2014) Amide proton transfer-weighted imaging of the head and neck at 3 T: a feasibility study on healthy human subjects and patients with head and neck cancer. NMR Biomed 27:1239–1247
25. By S, Barry RL, Smith AK, Lyttle BD, Box BA, Bagnato FR, Pawate S, Smith SA (2018) Amide proton transfer CEST of the cervical spinal cord in multiple sclerosis patients at 3T. Magn Reson Med 79:806–814
26. Dula AN, Pawate S, Dethrage LM, Conrad BN, Dewey BE, Barry RL, Smith SA (2016) Chemical exchange saturation transfer of the cervical spinal cord at 7 T. NMR Biomed 29:1249–1257
27. Wang J, Weygand J, Hwang KP, Mohamed ASR, Ding Y, Fuller CD, Lai SY, Frank SJ, Zhou J (2016) Magnetic resonance imaging of glucose uptake and metabolism in patients with head and neck cancer. Sci Rep 6:30618
28. Zhang S, Seiler S, Wang X, Madhuranthakam AJ, Keupp J, Knippa EE, Lenkinski RE, Vinogradov E (2018) CEST-Dixon for human breast lesion characterization at 3 T: a preliminary study. Magn Reson Med 80:895–903. https://doi.org/10.1002/mrm.27079
29. Schmidt H, Schwenzer NF, Gatidis S, Küstner T, Nikolaou K, Schick F, Martirosian P (2016) Systematic evaluation of amide proton chemical exchange saturation transfer at 3 T: effects of protein concentration, pH, and acquisition parameters. Investig Radiol 51:635–646
30. Zhou J, Payen JF, Wilson DA, Traystman RJ, van Zijl PCM (2003) Using the amide proton signals of intracellular proteins and peptides to detect pH effects in MRI. Nat Med 9:1085–1090
31. Zhou J, Tryggestad E, Wen Z et al (2010) Differentiation between glioma and radiation necrosis using molecular magnetic resonance imaging of endogenous proteins and peptides. Nat Med 17:130–134
32. Park KJ, Kim HS, Park JE, Shim WH, Kim SJ, Smith SA (2016) Added value of amide proton transfer imaging to conventional and perfusion MR imaging for evaluating the treatment response of newly diagnosed glioblastoma. Eur Radiol 26:4390–4403
33. Ma B, Blakeley JO, Hong X, Zhang H, Jiang S, Blair L, Zhang Y, Heo HY, Zhang M, van Zijl PCM, Zhou J (2016) Applying amide proton transfer-weighted MRI to distinguish pseudoprogression from true progression in malignant gliomas. J Magn Reson Imaging 44:456–462
34. Ohno Y, Kishida Y, Seki S et al (2017) Amide proton transfer-weighted imaging to differentiate malignant from benign pulmonary lesions: comparison with diffusion-weighted imaging and FDG-PET/CT. J Magn Reson Imaging 47:1013–1021
35. Jeong HK, Han K, Zhou J, Zhao Y, Choi YS, Lee SK, Ahn SS (2017) Characterizing amide proton transfer imaging in haemorrhage brain lesions using 3T MRI. Eur Radiol 27:1577–1584
36. Zhao X, Wen Z, Zhang G, Huang F, Lu S, Wang X, Hu S, Chen M, Zhou J (2013) Three-dimensional turbo-spin-echo amide proton transfer MR imaging at 3-Tesla and its application to high-grade human brain tumors. Mol Imaging Biol 15:114–122
37. Zhang XY, Wang F, Li H, Xu J, Gochberg DF, Gore JC, Zu Z (2017) Accuracy in the quantification of chemical exchange saturation transfer (CEST) and relayed nuclear Overhauser enhancement (rNOE) saturation transfer effects. NMR Biomed 30:e3716
38. Heo HY, Zhang Y, Lee DH, Hong X, Zhou J (2016) Quantitative assessment of amide proton transfer (APT) and nuclear overhauser enhancement (NOE) imaging with extrapolated semi-solid magnetization transfer reference (EMR) signals: application to a rat glioma model at 4.7 Tesla. Magn Reson Med 75:137–149